applied sciences

MDPI

Article

Fault-Tolerant Control for Carrier-Based Aircraft Based on Adaptive Fuzzy Sliding-Mode Method

Zhenlin Xing * and Jianliang Ai

Department of Aeronautics and Astronautics, Fudan University, Shanghai 200433, China; aijl@fudan.edu.cn
* Correspondence: 18110290005@fudan.edu.cn

Abstract: Carrier-based aircraft landing involves complex system engineering characterised by strong nonlinearity, significant coupling and susceptibility to environmental disturbances, and autonomous landing of carrier-based aircraft under fault states is even more challenging and riskier. To address the control-system problems of loss of efficiency and performance due to actuator faults and performance degradation due to various unknown disturbances, presented here is fault-tolerant control for carrier-based aircraft based on adaptive fuzzy sliding-mode fault-tolerant control (AFSMFTC). First, three models are built (the carrier-based aircraft fault model, the carrier air wake model and the deck motion model), and the control framework of the autonomous landing control system is introduced. Next, a longitudinal and lateral flight channel controller comprising an adaptive fuzzy network, adaptive laws and a sliding-mode controller is designed using the AFSMFTC method. The adaptive fuzzy network implements fuzzy approximation for the sliding-mode switching terms to further offset errors induced by unknown disturbances, the adaptive laws compensate for actuator faults, and the sliding-mode controller ensures tracking of the overall flight path. Furthermore, the stability of the fault-tolerant method is demonstrated using the Lyapunov function. Finally, simulation and comparative experiments show that the proposed fault-tolerant method has outstanding control performance and strong fault-tolerant capability, thereby providing an effective and feasible solution for designing an autonomous landing system for carrier-based aircraft under fault states.

Keywords: carrier-based aircraft; adaptive fuzzy control; sliding mode; fault-tolerant control

check for updates

Citation: Xing, Z.; Ai, J. Fault-Tolerant Control for Carrier-Based Aircraft Based on Adaptive Fuzzy Sliding-Mode Method. *Appl. Sci.* **2023**, *13*, 12685. https://doi.org/10.3390/app132312685

Academic Editor: Zhonghua Sun

Received: 6 October 2023
Revised: 22 November 2023
Accepted: 22 November 2023
Published: 26 November 2023

Copyright: © 2023 by the authors. Licensee MDPI, Basel, Switzerland. This article is an open access article distributed under the terms and conditions of the Creative Commons Attribution (CC BY) license (https://creativecommons.org/licenses/by/4.0/).

1. Introduction

The carrier strike group (CSG) is a vital part of modern marine military power, being an important foundation for a country to enhance its national defence capability and improve its international status. Meanwhile, carrier-based aircraft (CBA) play an important military role as crucial embodiments of air defence power in the CSG. Therefore, CBA landing technology has attracted widespread attention because it is a precondition for CBA to engage in actual marine combat [1–5]. Furthermore, the emergence of advanced multi-sensor navigation and localization algorithms [6–8] in recent years has provided significant support for research on CBA landing technology. Compared with land-based landing, the glide landing of CBA is extremely complex and difficult because of the limited dimensions of the carrier deck, the impacts of the marine environment and the characteristics of the inverse manoeuvring zone. Consequently, it is the stage with the highest accident rate in CBA operational missions. Early landing control technology was mainly based on classical control [9–11], but that could not give CBA favourable landing performance in a complex landing environment. Therefore, scholars have provided many methods for improvement based on modern control theory, such as fixed-time control [12,13], dynamic inversion control [14], fuzzy control [15,16], predictive control [17,18], sliding-mode control [19,20], backstepping control [21] and adaptive control [22,23]. However, all the aforementioned studies were based on the hypothesis that CBA remains in their normal states without any faults, whereas in reality, they are susceptible to combat damage and actuator faults due

to complex flight environments and large variations in dynamic pressure in operational missions, leading to serious degradation of system performance and posing direct threats to landing safety.

In light of the above, there is an urgent need to study fault-tolerant control (FTC) for CBA. In recent years, various FTC strategies based on advanced control theory have been applied increasingly to the design of flight controller subsystems because different models and relevant requirements of control quality are becoming increasingly complex, leading to visible achievements [24–26]. Sun et al. designed a fast adaptive terminal sliding-mode fault-tolerant controller for hypersonic flight vehicles to ensure limited state stability of the system with faults [27]. Gao et al. provided an observer-based passive FTC programme for the power system of near-space hypersonic flight vehicles with uncertain parameters and actuator faults [28]. Varal et al. designed a passive FTC method for unmanned aerial vehicles (UAVs) using dynamic inversion and robust integral technology of error signals to solve the efficacy failure of UAV actuators, and they proved the applicability of the method via simulations [29]. Xie et al. designed an FTC solution based on a linear active disturbance rejection controller to solve the loss fault of rudder surfaces on UAVs, and they realised effective compensation for faults [30]. Yang et al. designed an FTC strategy combined with an extended-state observer and sliding-mode control, which realised accurate compensation and effective control for carrier air wake turbulence via an extended-state observer; they also introduced a high-order linear differential tracker to obtain the required differential signals, and they verified it via simulation [31].

However, all the aforementioned studies were focused on passive FTC, which can reduce the sensitivity of the controlled system to faults by enhancing the robustness of the controller. Although neither fault diagnosis nor control reconstruction is needed, all types of possible faults must be known beforehand, which makes the controller relatively conservative and limited in its fault-tolerant function. By contrast, active FTC can reconfigure the control actions to actively counter faults in different components of the system [32,33]. However, the literature contains few relevant studies of landing control for CBA. In recent years, adaptive control theory has been applied widely to active FTC technology, and it has become a common theoretical method in FTC strategy after being combined with fuzzy theory [34], sliding-mode control theory [35,36], backstepping method [37], etc. Regarding establishing a fault-tolerant flight control system, modelling the controlled object and measuring uncertain parameters must be done first, and then the adaptiveness and robustness of the system should be ensured. Also, the problem of the large range of parameter fluctuations of the controlled object can be solved by using adaptive control theory, which is quite effective for ensuring the robustness of the controlled system.

Based on the characteristics of CBA landing, various unknown disturbances and possible actuator faults, presented herein is an FTC strategy based on adaptive fuzzy sliding-mode fault-tolerant control (AFSMFTC). The strategy involves using an adaptive fuzzy network to conduct fuzzy approximation for the sliding-mode switching terms, and it effectively weakens the impacts of unknown disturbances on the control system without estimating the upper limit of perturbation. Adaptive laws are used to counter the actuator efficiency loss fault, automatically adjust the controller parameters in the light of actuator faults and complete FTC under fault conditions, and a sliding-mode controller is used to ensure CBA tracking along the expected flight path. Finally, the applicability of the proposed method is verified by comparing it with the typical proportional–integral–derivative (PID) control method.

2. Mathematical Models

The six degrees of freedom (6DOF) nonlinear dynamics model and fault model of the CBA are described here for controller design.

2.1. Model of CBA

The equations of the 6DOF nonlinear model studied herein are presented below:

$$\begin{cases} \dot{x} = V\cos\gamma\cos\chi \\ \dot{y} = V\cos\gamma\sin\chi \\ \dot{z} = -V\sin\gamma \end{cases} \tag{1}$$

$$\begin{cases} \dot{u} = vr - wq - g\sin\theta + (F_x + T_x)/m \\ \dot{v} = -ur + wp + g\cos\theta\sin\phi + (F_x + T_x)/m \\ \dot{w} = uq - vp + g\cos\theta\cos\phi + (F_z + T_z)/m \end{cases} \tag{2}$$

$$\begin{cases} \dot{\phi} = p + (r\cos\phi + q\sin\phi)\tan\theta \\ \dot{\theta} = q\cos\phi - r\sin\phi \\ \dot{\beta} = p\sin\alpha - r\cos\alpha + \left(F_y + T_y\right)/mv \end{cases} \tag{3}$$

$$\begin{cases} \dot{p} = (c_1 r + c_2 p)q + c_3\overline{L} + c_4 N \\ \dot{q} = c_5 pr - c_6(p^2 - r^2) + c_7 M \\ \dot{r} = (c_8 p - c_2 r)q + c_4\overline{L} + c_9 N \end{cases} \tag{4}$$

Here, x_a, y_a and z_a are the positions of the CBA in the Earth-surface inertial reference frame; V, χ and γ are the ground velocity, flight-path azimuth angle and flight-path angle, respectively; m is the mass of the CBA; g is the acceleration due to gravity; u, v and w are the velocity components in the aircraft-body reference frame; α, β, ϕ and θ are the angle of attack, side-slip angle, roll angle and pitch angle, respectively; p, q and r are the rate of roll, rate of pitch and rate of yaw, respectively, in the aircraft-body reference frame; F_x, F_y and F_z are the aerodynamic components in the aircraft-body reference frame; T_x, T_y and T_z are the engine thrust components in the aircraft-body reference frame; and $\overline{L}$, M and N are the rolling moment, pitching moment and yawing moment, respectively, of the CBA in the aircraft-body reference frame.

Writing $x_1 = \begin{bmatrix}\phi & \theta & \beta\end{bmatrix}^T$ and $x_2 = \begin{bmatrix}p & q & r\end{bmatrix}^T$, Equations (3) and (4) become

$$\begin{cases} \dot{x}_1(t) = A + Bx_2(t) \\ \dot{x}_2(t) = F + Gu(t) \end{cases} \tag{5}$$

where $u = \begin{bmatrix}\delta_a & \delta_e & \delta_r\end{bmatrix}^T$ with δ_a, δ_e and δ_r being the aileron, elevator and rudder deflection angles, respectively, and A, B, F and G are parameter matrices of the CBA system. For specific details, which can be found in the reference [38].

2.2. Models of Faults and Disturbances

Various factors can induce actuator faults during CBA landing, also leading to landing failure. Common actuator faults are jamming, random drift, partial loss and saturation, and herein, the focus is mainly on partial loss [39], also known as efficiency loss. If this fault appears, then the actuator control directives experience deviations, leading to drops in gains, which further affect and weaken the actuator functions. Therefore, a partial-loss fault of an actuator can be described as

$$u_f(t) = \Lambda(t)u(t), t \geq t_f \tag{6}$$

where t_f is the time of failure and $\Lambda(t)$ is the loss coefficient matrix of the actuator. For the CBA discussed herein, the three types of actuators are those for the ailerons, elevators and rudder, and according we have $\Lambda(t) = diag(\rho_1(t), \rho_2(t), \rho_3(t))$, $0 < \rho_i < 1$.

In addition to actuator faults, this study also takes into account various unknown disturbances during CBA landing, including system perturbation, unmodelled dynamics and different environmental disturbances with adverse influences. These unknown disturbances are expressed by the following nonlinear function:

$$d(t, x_1, x_2) = \Delta A x_1 + \Delta B u + d_e = \begin{bmatrix}d_1 & d_2 & d_3\end{bmatrix}^T \tag{7}$$

where ΔA and ΔB are uncertain system parameters, d_e is the environmental disturbance, and $d_i < D, i = 1, 2, 3$, where D is a finite constant.

The above actuator-fault and disturbance models are substituted into Equation (5) to obtain the following CBA fault model:

$$\begin{cases} \dot{x}_1(t) = A + Bx_2(t) + d(t, x_1, x_2) \\ \dot{x}_2(t) = F + G\Lambda u(t) \end{cases} \tag{8}$$

The angular motion $x_1 = \begin{bmatrix} \phi & \theta & \beta \end{bmatrix}^T$ generally varies more slowly than does the angular velocity $x_2 = \begin{bmatrix} p & q & r \end{bmatrix}^T$, so time-scale separation theory is applicable here. This means that the CBA fault model can be considered as having a cascade system structure with two equations, so the command input in the first equation of (8) can be viewed as being a reference signal for the second equation.

3. Landing Environment

CBA landing is a complex process during which the CBA must traverse the airspace behind the carrier deck and eventually land on a runway of limited length, which is quite different from a land-based landing environment. During CBA landing, the flight altitude relative to sea level changes greatly. Also, the CBA is in the troposphere when it lands, where relatively significant airflow occurs, and the CBA is extremely susceptible to the carrier's air wake on approach and so is greatly challenged by the resulting complex aerodynamic environment. Finally, the flight deck experiences pitching, rolling and phugoid motions due to wind waves, so the ideal touchdown point thereon is a 6DOF spatial motion point, which can also seriously affect the landing safety.

3.1. Carrier Air Wake

In accordance with the United States Military Specification MIL-F-8785C, the carrier air wake can be considered as being a synthesis of random free atmospheric turbulence, a steady-state component, a periodic component and a random perturbation component [40], i.e.,

$$\begin{cases} u_w = u_1 + u_2 + u_3 + u_4 \\ v_w = v_1 + v_4 \\ w_w = w_1 + w_2 + w_3 + w_4 \end{cases} \tag{9}$$

where u_w, v_w and w_w are the horizontal–longitudinal, horizontal–lateral and vertical components of the carrier air wake, respectively, and the subscripts 1–4 represent random free atmospheric turbulence and the steady-state, periodic and random perturbation components of the carrier air wake, respectively.

3.2. Deck Motion

The 6DOF motion of the aircraft carrier under the impacts of wind and waves can be approximated as general rigid motion. The linear motions along the three axes are surge motion Δx_c, sway motion Δy_c and heave motion Δz_c, while the angular motions around the three axes are pitch motion θ_s, roll motion ϕ_c and yaw motion ψ_c. To simulate the aircraft carrier motion-triggered perturbation action, the theory of stationary random processes in reference [41] is cited here, and transfer functions are used to describe the deck motion, with the transfer functions of the aforementioned linear and angular motions expressed as

$$\begin{cases} G_T(s) = \frac{b_3 s^2 + b_2 s + b_1}{s^4 + a_4 s^3 + a_3 s^2 + a_2 s + a_1} \\ G_A(s) = \frac{d_3 s^2 + d_2 s + d_1}{s^4 + c_4 s^3 + c_3 s^2 + c_2 s + c_1} \end{cases} \tag{10}$$

The ideal touchdown point of the CBA is located between the second and third arresting cables in the middle landing runway on the carrier deck. Figure 1 shows the relationship between the ideal touchdown point and the carrier's centre of gravity.

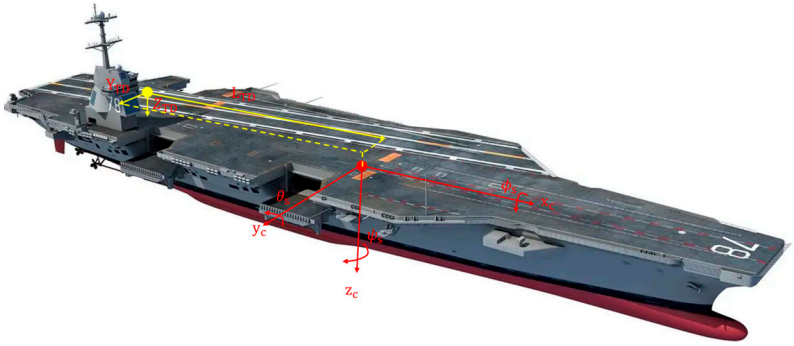


Figure 1. Relationship between centre of gravity of aircraft carrier and ideal touchdown point.

The causes of motion at the ideal touchdown point are divided into two parts, which are described in detail below:

$$\begin{cases} \Delta x_1 = \Delta x_c \cos\psi_c - \Delta y_c \sin\psi_c \\ \Delta y_1 = \Delta x_c \sin\psi_c + \Delta y_c \cos\psi_c \\ \Delta z_1 = \Delta z_c \end{cases} \tag{11}$$

$$\begin{cases} \Delta x_2 = -L_{TD}\cos\psi_c + L_{TD} - Y_{TD}\sin\psi_c - Z_{TD}\sin\theta_c\cos\psi_c \\ \Delta y_2 = -L_{TD}\sin\psi_c - Y_{TD} + Y_{TD}\cos\psi_c + Z_{TD}\sin\phi_c\cos\psi_c \\ \Delta z_2 = L_{TD}\sin\theta_s + Y_{TD}\sin\phi_c - Z_{TD}\sin\phi_c\cos\theta_c + Z_{TD} \end{cases} \tag{12}$$

where $[\Delta x_1, \Delta y_1, \Delta z_1]$ and $[\Delta x_2, \Delta y_2, \Delta z_2]$ are formed by the aforementioned linear and angular motions along the carrier deck, respectively, and $[L_{TD}, Y_{TD}, Z_{TD}]$ is the distance vector between the ideal touchdown point and the centre of gravity of the deck. Therefore, the ideal touchdown point can be expressed as

$$\begin{cases} x_p = V_c t\cos(\psi_c + \psi_0) + \Delta x_1 + \Delta x_2 \\ y_p = V_c t\sin(\psi_c + \psi_0) + \Delta y_1 + \Delta y_2 \\ z_p = \Delta z_1 + \Delta z_2 \end{cases} \tag{13}$$

where V_c is the cruising speed of the aircraft carrier, ψ_c (=0°) is its heading angle and ψ_0 is the angle between the carrier's cruising direction and deck centre line.

3.3. Autonomous Carrier Landing System (ACLS) Control Framework

The CBA is susceptible to external disturbances, such as the carrier air wake and sea wind and waves during landing, and to unfavourable conditions, such as actuator faults, leading to reduced or even unstable control performance. To avoid unfavourable conditions, ensure landing safety and improve the landing success rate, an ACLS must be developed for the CBA to track the reference path accurately and quickly, thereby providing support for the CBA to reach the ideal touchdown point.

ACLS is targeted at correcting the initial position, controlling the perturbations from the carrier air wake, tracking the glide path and effectively solving the fault-induced degradation problems of the control system. As shown in Figure 2, its control framework comprises a glide-path generation subsystem, a guidance subsystem, a flight controller subsystem and an aircraft-fault subsystem.

The function of the glide-path generation subsystem is to collect the longitudinal and lateral errors between the CBA and the expected glide path. The ideal touchdown point on the carrier deck is a 6DOF spatial motion point because of the impact of complex sea conditions, while the expected glide path. The ideal touchdown point on the carrier deck is a 6DOF spatial motion point because of the impact of complex sea conditions, while the expected glide path is directly affected by the ideal touchdown point. Therefore, there is a need to build a relative positional relationship between the CBA and the ideal touchdown point. The centre-of-gravity position of the CBA is defined as (x_a, y_a, z_a), while the ideal touchdown point is defined as (x_c, y_c, z_c). Therefore, the relative positional relationship between the CBA and the aircraft carrier is described as

$$\begin{bmatrix} x_r \\ y_r \\ z_r \end{bmatrix} = L_{cg} \begin{bmatrix} x_a - x_p \\ y_a - y_p \\ z_a - z_p \end{bmatrix} \tag{14}$$

where L_{cg} is the transfer matrix from the Earth-surface inertial reference frame to the motion reference frame of the aircraft carrier.

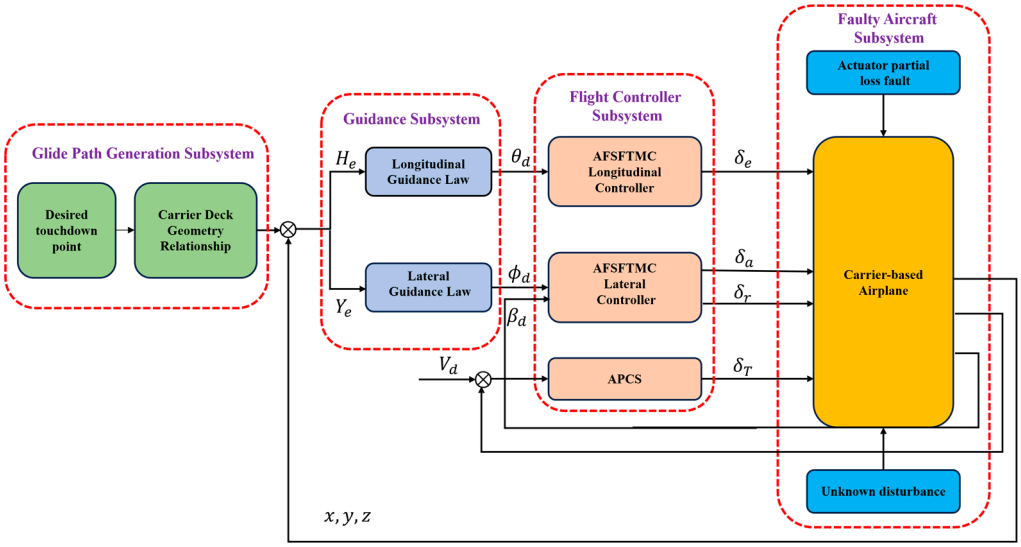


Figure 2. ACLS Control Framework.

Figure 3 shows the positional relationship between the CBA and the ideal touchdown point, where γ_p is the expected glide-path angle and σ_p is the angle between the expected glide path and the aircraft carrier. Therefore, the path-tracking error is obtained as

$$\begin{bmatrix} H_e \\ Y_e \end{bmatrix} = \begin{bmatrix} z_r - x_r \tan \sigma_p \\ y_r \end{bmatrix} \tag{15}$$

$$\tan \sigma_p = \frac{\sin \gamma_p}{\cos \gamma_p - V_a / V_c} \tag{16}$$

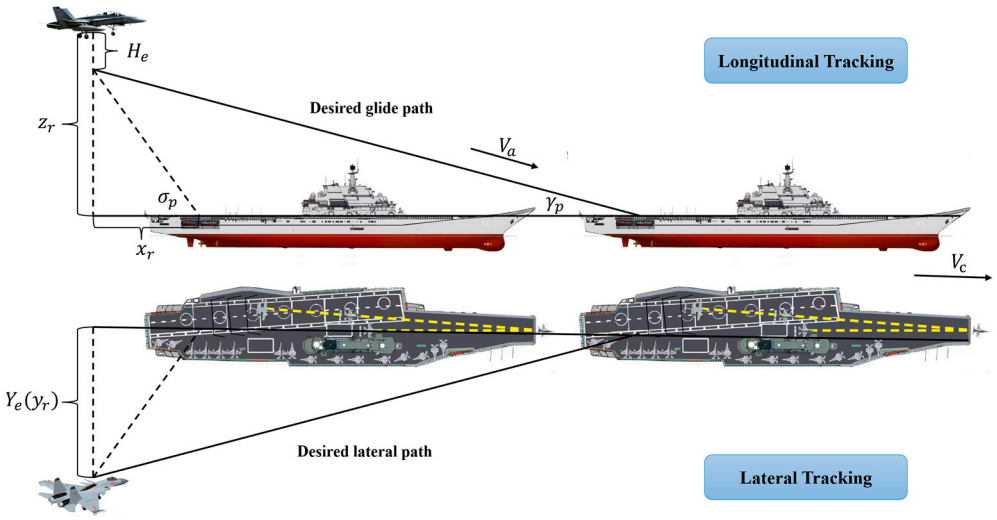


Figure 3. Diagram of CBA landing.

The function of the guidance subsystem is to transform position errors into angular commands to control the angular variations. The guidance subsystem is generally divided

into a longitudinal channel and a lateral channel. The longitudinal channel selects the path controller containing a $\sigma - \beta$ filter to transform flight altitude tracking commands into a pitch angle control command θ_d, while the lateral channel uses PID control to transform lateral deviations into the expected side-slip angle β_d and roll angle ϕ_d. The two input terms in the aircraft-fault subsystem are actuator fault and unknown disturbance, the occurrence times of which are indefinite. If unknown faults is added, the CBA cannot steadily track the glide path, leading to significant influences on landing safety and success rate. Therefore, there is necessary to develop an effective fault-tolerant flight system to address the fault-induced uncertainties.

The flight controller subsystem comprises an approach power compensator system (APCS), a longitudinal flight controller subsystem and a lateral flight controller subsystem. The function of APCS is to keep the angle of attack or velocity constant via autothrottle control in order to directly transform variations in pitch angle into variations in flight-path angle and enhance the flight-path control characteristic of the CBA during glide and landing. Consequently, the flight-path control performance of the CBA can be improved. This study directs the APCS controller to output the appropriate δ_T to keep the velocity constant. Meanwhile, the function of AFSMFTC is to complete the tracking and control for the expected attitude angle by controlling δ_a, δ_e and δ_r. To eliminate the influences of adverse factors on the control effects, an adaptive function and a sliding-mode fuzzy controller are designed in this study to compensate for the efficiency and performance loss of actuators and various unknown perturbations, respectively.

4. Control Strategy

This section describes in detail the AFSMFTC design, selects the adaptive fuzzy system to weaken errors induced by external disturbances and proposes switching terms in the sliding-mode controller to effectively reduce buffeting on rudder surfaces. The adaptive fuzzy laws are derived by the Lyapunov algorithm to ensure stability and convergence of the whole closed-loop system by adjusting the adaptive weights. Moreover, the APCS design method is also described briefly.

4.1. Design of AFSMFTC

As mentioned above, the collected flight-path tracking errors can be transformed into attitude control commands with the assistance of the glide-path generation subsystem and the guidance subsystem. Consequently, the landing control problem can be transformed into an attitude control problem. The AFSMFTC structure is shown in Figure 4.

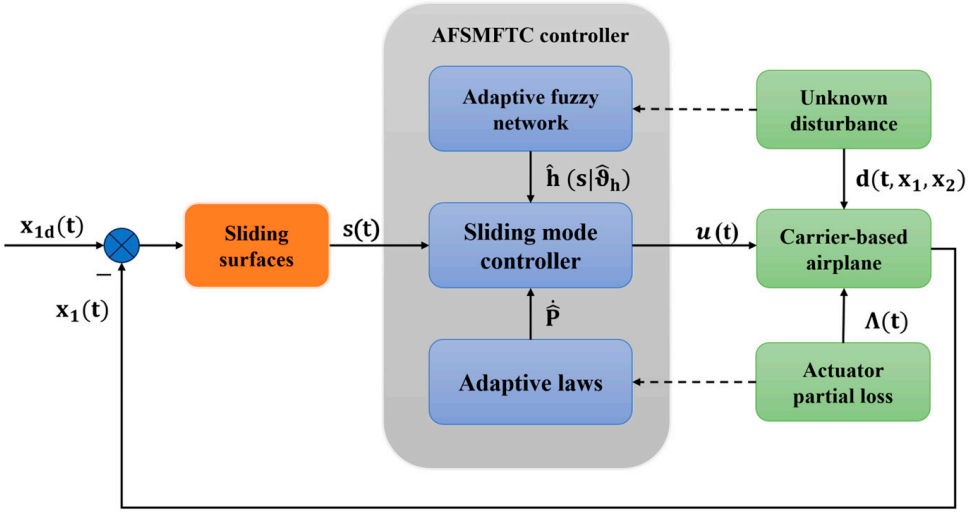


Figure 4. AFSMFTC Structure.

Letting the control command for the expected attitude angle be $x_{1d} = \begin{bmatrix} \phi_d & \theta_d & \beta_d \end{bmatrix}^T$, the state-tracking error can be defined as

$$e_1(t) = x_1(t) - x_{1d}(t) \tag{17}$$

The sliding-mode switching function is designed as

$$s_1(t) = e_1(t) + c_1 \int_0^t e_1(t)dt \tag{18}$$

Meanwhile, the sliding-mode control law is designed as

$$x_2 = B^{-1}\left(-A + \dot{x}_{1d} - c_1 e_1 - \eta \mathrm{sgn}(s_1)\right) \tag{19}$$

where $\eta \geq |d(t, x_1, x_2)|$, the proof of the invertibility of B is provided in reference [35].

In addition, it is difficult to measure the upper limit of unknown perturbations during real-world CBA landing because of the complex and random landing environment. Therefore, this study further designs adaptive fuzzy sliding-mode control laws to offset errors induced by unknown disturbances without an upper perturbation limit; switching terms are substituted by consecutive fuzzy systems, which can effectively reduce buffeting on rudder surfaces, and $\hat{h}(s_1)$ is selected and used to approximate $\eta \mathrm{sgn}(s_1)$.

The fuzzy system is constructed in accordance with fuzzy rules in the form of an IF-THEN statement:

$$R^{(l)}: \text{IF } s_i \text{ is } A_1^l \text{ and } \cdots \text{and } s_i^{(n)} \text{ is } A_n^l$$
$$\text{THEN } h_i \text{ is } B_i^l$$

where n is the order of the derivative s_i. A product inference engine, single-value defuzzifier and centre-average defuzzifier are used to output the fuzzy system as

$$h_i = \frac{\sum_{l=1}^{N} q_i^l \left(\prod_{n}^{k=1} \mu_{A_k^l}(x_k) \right)}{\sum_{l=1}^{N} \left(\prod_{n}^{k=1} \mu_{A_k^l}(x_k) \right)} \tag{20}$$

where $\mu_{A_k^l}(x_k)$ is the membership function of x_k.

The vector $\xi(x)$ is introduced. Let $\xi(x) = (\xi_1, \xi_2, \cdots, \xi_N)^T$, where

$$\xi_l = \frac{\prod_{n}^{k=1} \mu_{A_k^l}(x_k)}{\sum_{l=1}^{N} \left(\prod_{n}^{k=1} \mu_{A_k^l}(x_k) \right)} \tag{21}$$

Then $h_i(x) = \vartheta_i^T \xi(x)$ and $\vartheta_i = [q_i^1, \cdots q_i^N]^T$ can be obtained. Let $\hat{h}(s|\vartheta_h) = (\vartheta_h^T \xi(s))^T$, then $\vartheta_h = [\vartheta_1 \ \vartheta_2 \ \vartheta_3]^T$, where ϑ_h varies in accordance with the adaptive laws. The network structure of the adaptive fuzzy system is shown in Figure 5.

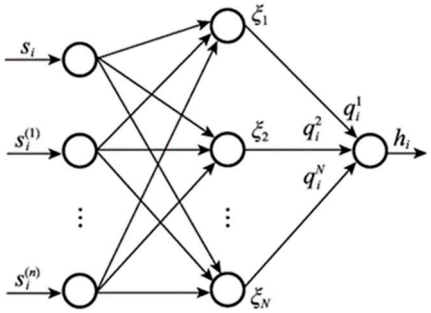


Figure 5. Network Structure of Adaptive Fuzzy System.

The control law (19) is transformed into

$$x_2 = B^{-1}\left(-A + \dot{x}_{1d} - c_1 e_1 - \hat{h}(s_1)\right) \tag{22}$$

$$\hat{h}(s|\hat{\vartheta}_h) = \hat{\vartheta}_h^T \xi(s) \tag{23}$$

where $\hat{h}(s|\hat{\vartheta}_h)$ is the output of the fuzzy system, $\xi(s)$ is the fuzzy vector, and the vector $\hat{\vartheta}_h^T$ varies in accordance with the adaptive laws.

The optimal parameter is defined as

$$\vartheta_h^* = \arg\min_{\hat{\vartheta}_h \in \Omega_h} [\sup|h(s|\hat{\vartheta}_h) - \eta \mathrm{sgn}(s)|] \tag{24}$$

where ϑ_h^* is the variable value when minimum values of the object function are taken, and Ω_h is the set of $\hat{\vartheta}_h$. Let

$$\hat{h}(s|\vartheta_h^*) = \eta \mathrm{sgn}(s) \tag{25}$$

where $\eta \geq |d(t, x_1, x_2)|$. The adaptive control law is designed as

$$\dot{\hat{\vartheta}}_h = \gamma s \xi(s) \tag{26}$$

where $\gamma > 0$.

Theorem 1. *If the control law* $x_2 = B^{-1}\left(-A + \dot{x}_{1d} - c_1 e_1 - \hat{h}(s_1)\right)$ *is used, then the first equation in the closed-loop system (8) is stable, and the tracking error* e_1*converges to zero in a limited time.*

Proof 1. We have

$$\begin{aligned} \dot{s}_1 &= \dot{e} + c_1 \dot{e} = \dot{x}_1 - \dot{x}_{1d} + c_1 \dot{e} \\ &= A + B x_2 + d - \dot{x}_{1d} + c_1 \dot{e} \\ &= -\hat{h}(s|\hat{\vartheta}_h) + d + \hat{h}(s|\vartheta_h^*) - \hat{h}(s|\vartheta_h^*) \\ &= \tilde{\vartheta}_h^T \xi(s) + d - \hat{h}(s|\vartheta_h^*) \end{aligned} \tag{27}$$

where $\tilde{\vartheta}_h = \vartheta_h^* - \hat{\vartheta}_h$. The Lyapunov function is defined as

$$V_1 = \frac{1}{2}\left(s_1^T s_1 + \frac{1}{\gamma}\tilde{\vartheta}_h^T \tilde{\vartheta}_h\right) \tag{28}$$

and the derivative of V_1 is taken as

$$\begin{aligned} \dot{V}_1 &= s_1^T \dot{s}_1 + \tfrac{1}{\gamma}\tilde{\vartheta}_h^T \dot{\tilde{\vartheta}}_h \\ &= s_1^T (\tilde{\vartheta}_h^T \xi(s) + d - \hat{h}(s|\vartheta_h^*)) + \tfrac{1}{\gamma}\tilde{\vartheta}_h^T \dot{\tilde{\vartheta}}_h \end{aligned} \tag{29}$$

For $\dot{\tilde{\vartheta}}_h = -\dot{\hat{\vartheta}}_h$, the ideal output $\hat{h}(s|\vartheta_h^*) = \eta \mathrm{sgn}(s)$ and the adaptive law $\dot{\hat{\vartheta}}_h = \gamma s \xi(s)$ are substituted into Equation (29) to obtain

$$\begin{aligned} \dot{V}_1 &= \tfrac{1}{\gamma}\tilde{\vartheta}_h^T (\gamma s_1 \xi(s) + \dot{\tilde{\vartheta}}_h) + d s_1 - s_1 \eta \mathrm{sgn}(s_1) \\ &= \tfrac{1}{\gamma}\tilde{\vartheta}_h^T (\gamma s_1 \xi(s) - \dot{\hat{\vartheta}}_h) + d s_1 - \eta |s_1| \\ &= d s_1 - \eta |s_1| \leq 0 \end{aligned} \tag{30}$$

When $\dot{V} \equiv 0$ and $s \equiv 0$, according to the LaSalle invariant set theorem, if $t \to \infty$, then $e_1 \to 0$. Hence, Theorem 1 is proved to be true.

According to the second equation $\dot{x}_2(t) = F + G\Lambda u(t)$ in Equation (8), the expected control command is $x_{2d} = x_2 = B^{-1}\left(-A + \dot{x}_{1d} - c_1 e_1 - \hat{h}(s_1)\right)$, and the state tracking error is defined as

$$e_2(t) = x_2(t) - x_{2d}(t) \tag{31}$$

The sliding-mode switching function is designed as

$$s_2(t) = e_2(t) + c_2 \int_0^t e_2(t)dt \tag{32}$$

and the derivative of $s_2(t)$ is taken as

$$\dot{s}_2 = \dot{e}_2 + c_2 e_2 = \dot{x}_2 - \dot{x}_{2d} + c_2 e_2 \tag{33}$$

The equation $\dot{x}_2(t) = F + G\Lambda u(t)$ is substituted into Equation (33) to obtain

$$\dot{s}_2 = F + G\Lambda u(t) - \dot{x}_{2d} + c_2 e_2 \tag{34}$$

If $\mathrm{P} = (G\Lambda)^{-1}$, $\lambda = F + ks_2 + c_2 e_2 - \dot{x}_{2d} + \varepsilon \mathrm{sgn}(s_2)$ and the estimated value of P is defined as $\hat{\mathrm{P}}$, then the error of estimate is $\widetilde{\mathrm{P}} = \mathrm{P} - \hat{\mathrm{P}}$. The control law and adaptive law are designed as

$$u = -\hat{\mathrm{P}}\lambda \tag{35}$$

$$\dot{\hat{\mathrm{P}}} = \kappa s_2^T \lambda \mathrm{sgn}(G) \tag{36}$$

□

Theorem 2. *If the control law $u = -\hat{\mathrm{P}}\lambda$ is used, then the second equation in the closed-loop system (8) is stable, and the tracking error e_2 converges to zero in a limited time. This also means that the aircraft-fault subsystem is progressively stable.*

Proof 2. The Lyapunov function is defined as

$$V_2 = \frac{1}{2}\left(s_2^T s_2 + \frac{|G\Lambda|}{\kappa}\widetilde{\mathrm{P}}^T\widetilde{\mathrm{P}}\right) \tag{37}$$

and the derivative of V_2 is taken as

$$\dot{V}_2 = s_2^T \dot{s}_2 + \frac{|G\Lambda|}{\kappa}\widetilde{\mathrm{P}}^T\dot{\widetilde{\mathrm{P}}} \tag{38}$$

Equations (34) and (35) are substituted into Equation (38) to obtain

$$\begin{aligned} \dot{V}_2 &= s_2^T(F + G\Lambda u - \dot{x}_{2d} + c_2 e_2) + \tfrac{|G\Lambda|}{\kappa}\widetilde{\mathrm{P}}^T\dot{\widetilde{\mathrm{P}}} \\ &= s_2^T(G\Lambda u + \lambda - ks_2 - \varepsilon \mathrm{sgn}(s_2)) + \tfrac{|G\Lambda|}{\kappa}\widetilde{\mathrm{P}}^T\dot{\widetilde{\mathrm{P}}} \\ &= s_2^T(-G\Lambda\hat{\mathrm{P}}\lambda + \lambda - ks_2 - \varepsilon \mathrm{sgn}(s_2)) + \tfrac{|G\Lambda|}{\kappa}\widetilde{\mathrm{P}}^T\dot{\widetilde{\mathrm{P}}} \end{aligned} \tag{39}$$

For $\mathrm{sgn}(G) = \mathrm{sgn}(G\Lambda)$, the adaptive law $\dot{\hat{\mathrm{P}}} = \kappa s_2^T \lambda \mathrm{sgn}(G)$ is substituted into Equation (39) to obtain

$$\begin{aligned} \dot{V}_2 &= s_2^T(-G\Lambda\hat{\mathrm{P}}\lambda + \lambda - ks_2 - \varepsilon \mathrm{sgn}(s_2)) + |G\Lambda|\widetilde{\mathrm{P}}^T s_2^T \lambda \mathrm{sgn}(G) \\ &= s_2^T(-G\Lambda\hat{\mathrm{P}}\lambda + \lambda - ks_2 - \varepsilon \mathrm{sgn}(s_2) + G\Lambda\widetilde{\mathrm{P}}^T\lambda) \\ &= s_2^T(-G\Lambda\mathrm{P}\lambda + \lambda - ks_2 - \varepsilon \mathrm{sgn}(s_2)) \\ &= s_2^T(-ks_2 - \varepsilon \mathrm{sgn}(s_2)) \\ &= -ks_2^2 - \varepsilon|s_2| \le 0 \end{aligned} \tag{40}$$

According to the LaSalle invariant set theorem, if $t \to \infty$, then $e_2 \to 0$. Hence, Theorem 2 is proved to be true.

In summary, the AFSMFTC method is designed as follows:

$$\begin{cases} x_2 = B^{-1}\left(-A + \dot{x}_{1d} - c_1 e_1 - \hat{h}(s_1)\right) \\ u = -\hat{\mathrm{P}}\lambda = -\hat{\mathrm{P}}\left(F + ks_2 + c_2 e_2 - \dot{x}_{2d} + \varepsilon \mathrm{sgn}(s_2)\right) \end{cases} \tag{41}$$

To effectively weaken buffeting, the saturation function $sat(s)$ substitutes the sign function $\mathrm{sgn}(s)$, i.e.,

$$sat(s) = \begin{cases} 1 & s > \Delta \\ ks & |s| \leq \Delta \\ -1 & s < -\Delta \end{cases} \tag{42}$$

where $k = 1/\Delta$ and Δ is the boundary layer. □

The essence of using sliding-mode control of the saturation function is that switching control is applied outside the boundary layer so that the system state quickly approaches the sliding mode, while feedback control is applied inside the boundary layer to reduce the buffeting resulting from fast switching of the sliding mode and to ensure that the function s is long kept inside the boundary layer.

4.2. Design of APCS

If the CBA is not equipped with APCS when ACLS is working, then its manoeuvring performance is weakened under low dynamic pressure during landing, leading to an inability to track variations in attitude angle through the flight-path angle and to control the flight path. Using the constant-velocity APCS control programme means adding the velocity stability derivative of the CBA, which further effectively controls velocity variations induced by variations in attitude angle and improves the damping of long periodic motion.

The velocity tracking error is defined as

$$e_v = V - V_d \tag{43}$$

where V_d is the expected flight speed. Hence, the APCS control law is expressed as

$$\delta_T = K_{P_V} e_V + K_{I_V} \int e_V \tag{44}$$

where K_{P_V} and K_{I_V} are constant gains.

5. Simulation Results

Before conducting simulation validation, it is necessary to study the choice of gain values in the sliding mode controller. The specific selection of gain values for a sliding mode controller is influenced by factors such as system characteristics, control requirements, and operating conditions. In generally, the range of sliding mode gain values should be adjusted appropriately. Increasing the sliding mode gain can improve the system's sensitivity and response speed but may lead to chattering and instability. Therefore, within the range of gain values, it is important to ensure that it does not exceed the system's tolerance for chattering and prevent the occurrence of instability. Reducing the sliding mode gain can enhance system stability and reduce chattering but may sacrifice dynamic performance and response speed. Thus, when determining the range of gain values, a balance between stability and performance needs to be found.

The specific range of sliding mode gain values is typically determined based on the specific system and can be adjusted and optimized through methods such as experimentation, simulation, and empirical analysis. It is important to select gain values that meet the control requirements of the system while maintaining stability and performance. In comparison to the commonly used trail-and-error method and parameter optimization methods, this paper adopts the trail-and-error method to obtain a suitable range of sliding mode gains, as shown in Table 1.

When the sliding mode gain parameter is within the reference range mentioned in Table 1, the system exhibits good dynamic and steady-state characteristics. If the value is lower than the reference range, the dynamic response speed of the system will decrease. Similarly, if the value exceeds the reference range, the steady-state characteristics of the system weaken, leading to oscillations.

Table 1. Selection of the sliding mode gain range.

Sliding Mode Gain Parameter	Reference Value Range
c_ϕ	[5,10]
c_θ	[5,11]
c_β	[7,13]
c_p	[8,17]
c_q	[6,12]
c_r	[8,15]

To verify the applicability of the proposed AFSMFTC-based autonomous landing system, various simulations and comparative experiments are presented below.

An F/A-18A CBA is selected as the object in this study, the model parameters of which are listed in reference [42]. The initial position of the CBA and the ideal touchdown point on the carrier deck are (0, 5, 210) m and (0, 2500, 10.8) m, respectively, and the initial state parameters are $\phi_0 = 0^\circ$, $\theta_0 = 4.6^\circ$, $\alpha_0 = 8.1^\circ$, $\beta_0 = 0^\circ$, $V_a = 70$ m/s and $V_c = 12.86$ m/s. The settings of the controller parameters include the sliding-mode surface parameters $c_1 = diag(8, 8, 10)$ and $c_2 = diag(12, 10, 12)$, the adaptive-law parameters $\kappa = 0.8$, $\lambda = 1.5$ and $\gamma = 10$ and the fuzzy-controller membership functions $\mu_N(s) = \frac{1}{1+\exp(5(s+3))}$, $\mu_Z(s) = \exp(-s^2)$, $\mu_P(s) = \frac{1}{1+\exp(5(s-3))}$ and $\hat{\vartheta}_h^T = [0.1, 0.1, 0.1]^T$.

5.1. Simulation 1

To showcase the performance of the designed AFSMFTC method in inner-loop tracking, the pitch angle is taken as an example. The validation is conducted using a unit step signal and a sinusoidal signal. Additionally, a comparison is made with the active disturbance rejection control (ADRC) method, incremental nonlinear dynamic inversion (INDI) method, and conventional PID method mentioned in the references [43,44]. The simulation results are shown in Figure 6.

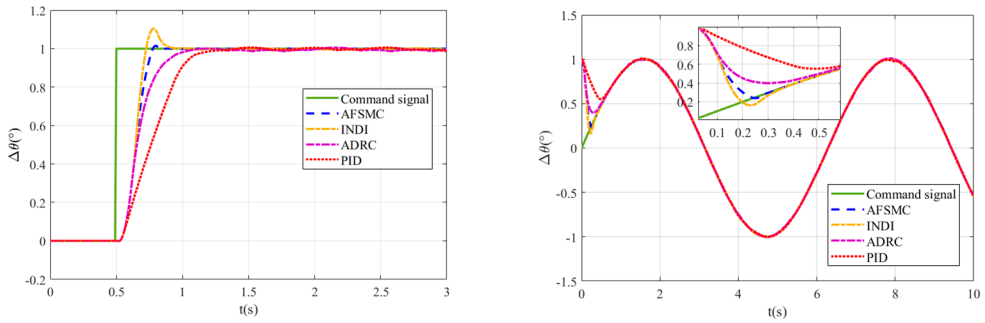


Figure 6. Response curves of pitch angle: (**a**) Response curves of pitch angle under the step signal; (**b**) Response curves of pitch angle under the sinusoidal signal.

From Figure 6, it can be observed that the AFSMFTC method designed in this study achieves the desired state faster compared to other methods. Additionally, it exhibits smaller overshoot during the tracking process, demonstrating excellent dynamic characteristics and robustness.

5.2. Simulation 2

Next, the superiority of the designed AFSMFTC method over the conventional PID method in tracking and anti-disturbance performance in a normal landing is verified via the simulation results shown in Figures 7–9.

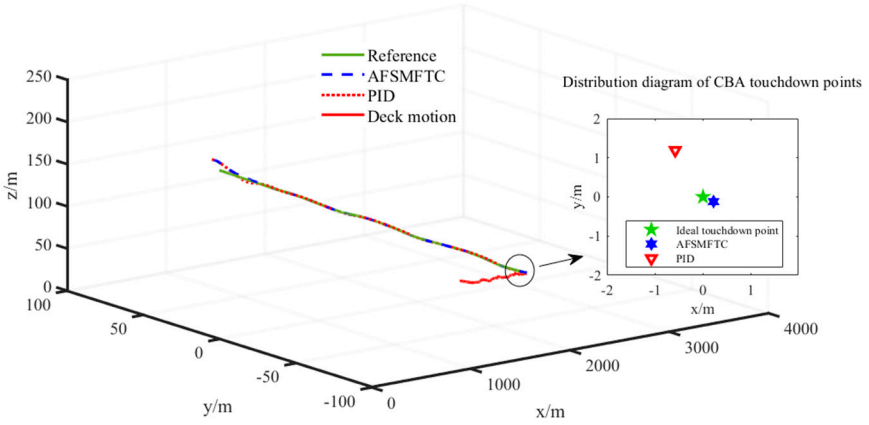
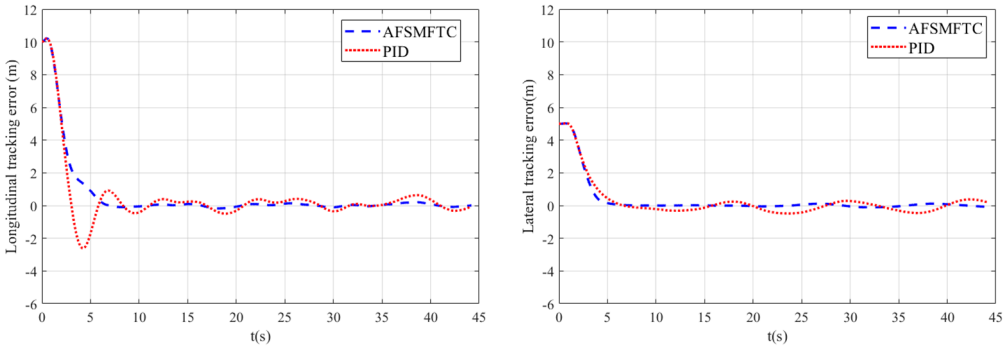


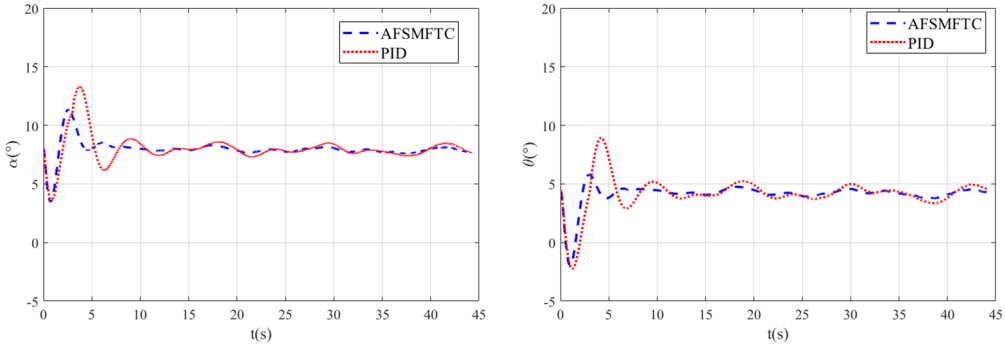
Figure 7. Landing Path of CBA.



(**a**) (**b**)

Figure 8. Landing path tracking of CBA in normal state: (**a**) Longitudinal tracking error; (**b**) Lateral tracking error.

Figures 8 and 9 show curves of the 3D path and position errors, respectively, of the CBA in a normal landing. As can be seen, the PID method shows distinct error fluctuations in the longitudinal and lateral directions, although it can still complete a normal landing. By contrast, the proposed AFSMFTC-based ACLS synchronously tracks the deck motion faster and more accurately and almost avoids the impacts of the carrier air wake, thereby improving the tracking performance.



(**a**) (**b**)

Figure 9. *Cont.*

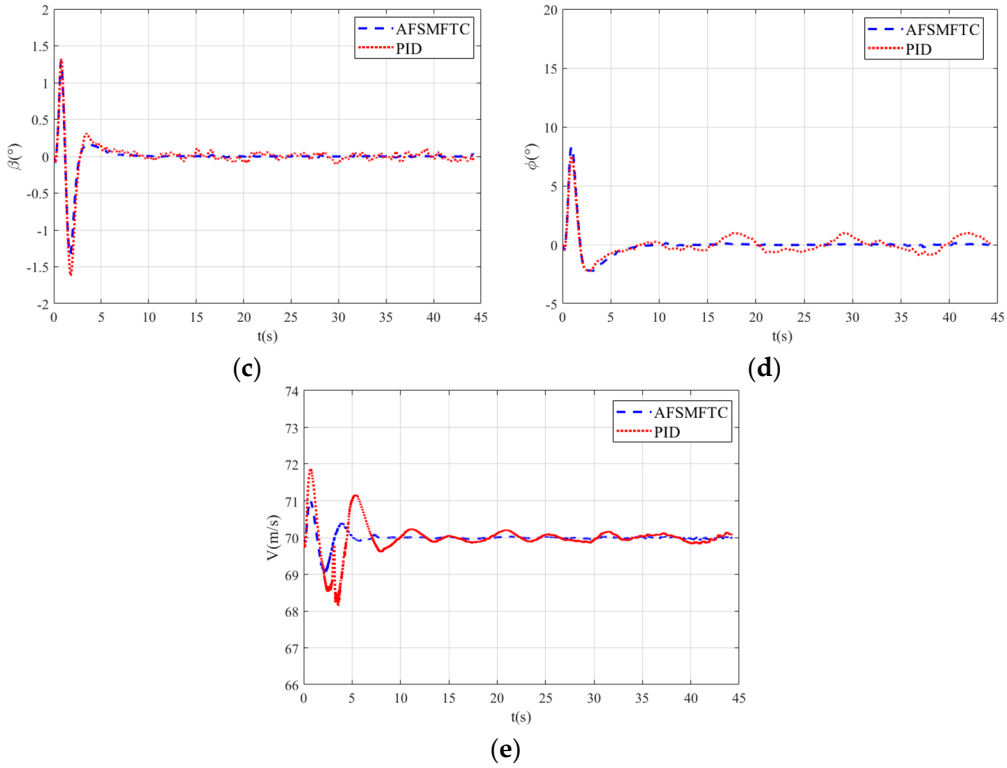


Figure 9. Response curves of flight variables of CBA in normal state: (**a**) Angle of attack; (**b**) Pitch angle; (**c**) Side-slip angle; (**d**) Roll angle; (**e**) Velocity.

Furthermore, the impact of the carrier air wake in the longitudinal direction on the landing performance of the CBA is far higher than that in the lateral direction during a normal landing, as shown in Figure 9. Therefore, the AFSMFTC-based ACLS method is distinctly superior to the conventional PID method in controlling the angle of attack, pitch angle and airspeed in the longitudinal direction, and it is more capable of keeping the angle of attack, velocity and pitch angle in smaller fluctuation ranges. However, the two methods differ less in the lateral direction.

5.3. Simulation 3

To further verify the aforementioned anti-disturbance performance of the AFSMFTC method, unknown disturbances consisting of system parameter perturbations and external disturbances are introduced at 2 s after the beginning of a normal CBA landing. The unknown disturbances are described as

$$d(t, x_1, x_2) = \begin{bmatrix} 0.3(p+\phi) + 0.05sint \\ 0.25(q+\theta) + 0.2sint \\ 0.2(r+\beta) + 0.1sint \end{bmatrix} \tag{45}$$

The simulation results are shown in Figures 10 and 11.

Figure 10 shows that the conventional PID method cannot adjust the control parameters in real time after the introduction of disturbance signals; rather, it progressively generates divergent phenomena that eventually result in the CBA being uncontrollable. By contrast, the proposed AFSMFTC method approaches the boundary of unknown disturbances through an adaptive fuzzy sliding-mode controller and ensures that the CBA still has good path-tracking performance under various disturbances.

Figure 11 shows that introducing unknown disturbances affects different flight state variables of the CBA from time to time, but different attitude angles and velocities can still be maintained in a small range of fluctuation, indicating good anti-disturbance capability of the AFSMFTC method.

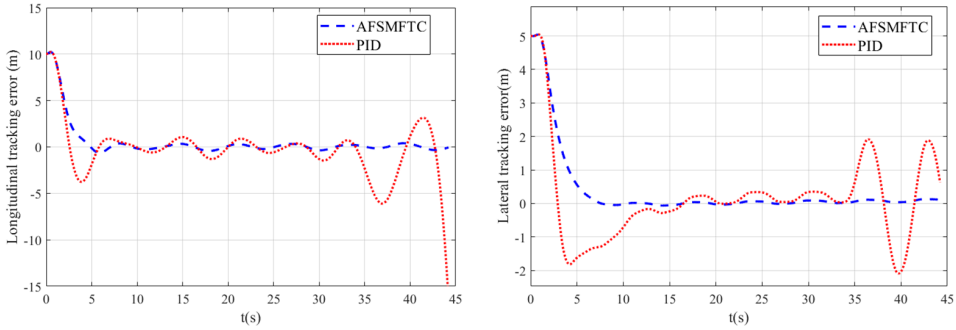


Figure 10. Landing path tracking of CBA under unknown disturbances: (**a**) Longitudinal tracking error; (**b**) Lateral tracking error.

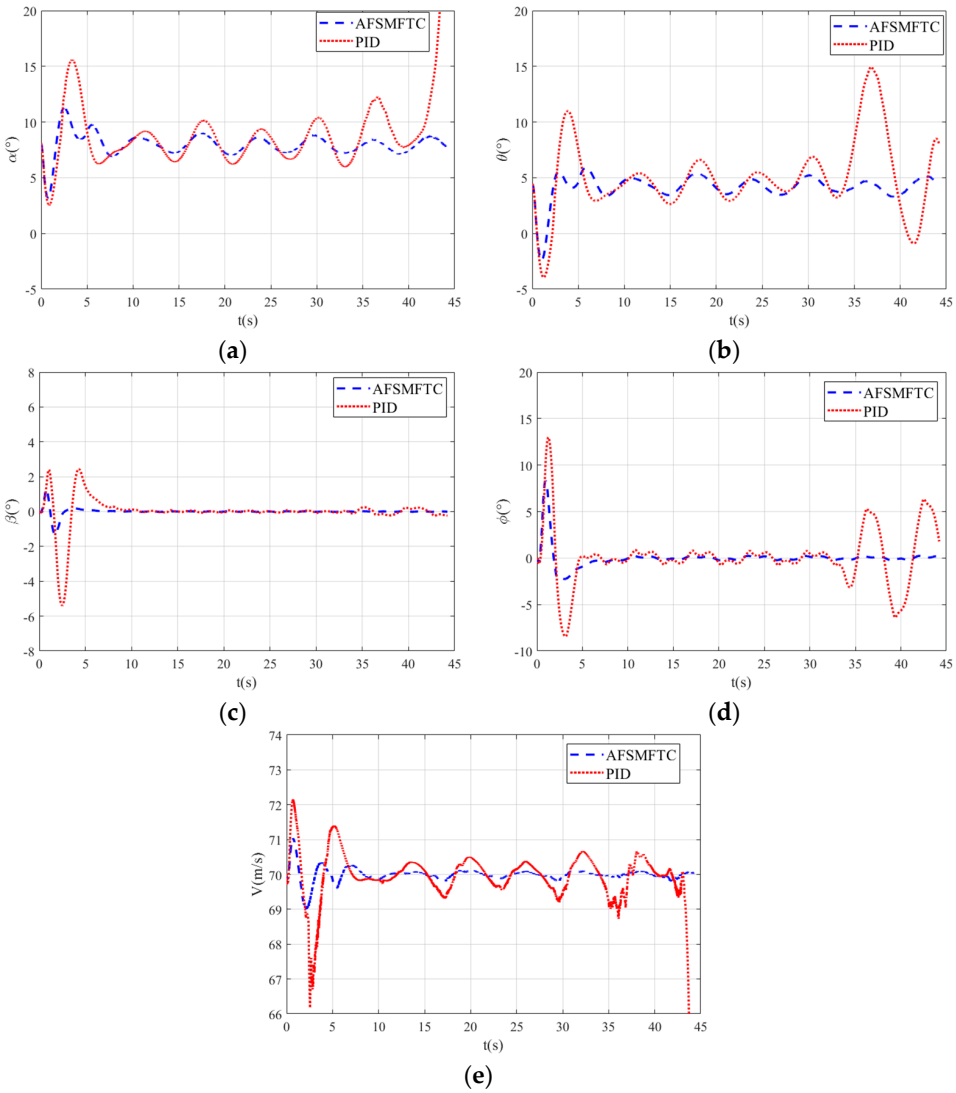


Figure 11. Response curves of flight variables of CBA under unknown disturbances: (**a**) Angle of attack; (**b**) Pitch angle; (**c**) Side-slip angle; (**d**) Roll angle; (**e**) Velocity.

5.4. Simulation 4

To further verify the applicability of the AFSMFTC method under actuator faults, an actuator efficiency loss fault is introduced at 2 s after the beginning of a normal CBA landing. The actuator efficiency loss matrix is described as

$$\Lambda(t) = diag(0.5, 0.5, 0.5) \tag{46}$$

The simulation results are shown in Figures 12 and 13.

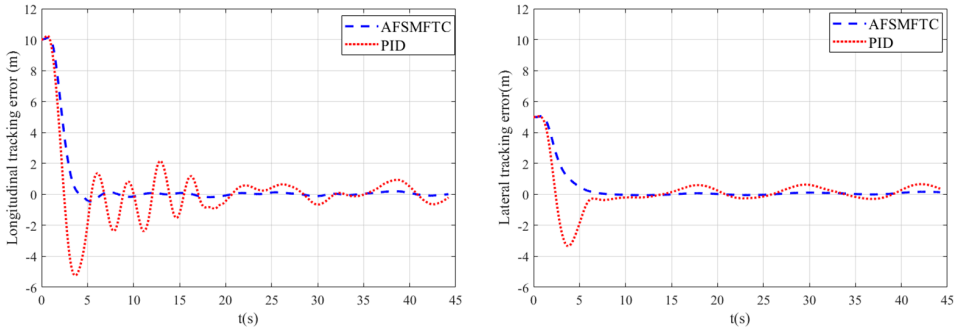


Figure 12. Landing path tracking of CBA under actuator faults: (**a**) Longitudinal tracking error; (**b**) Lateral tracking error.

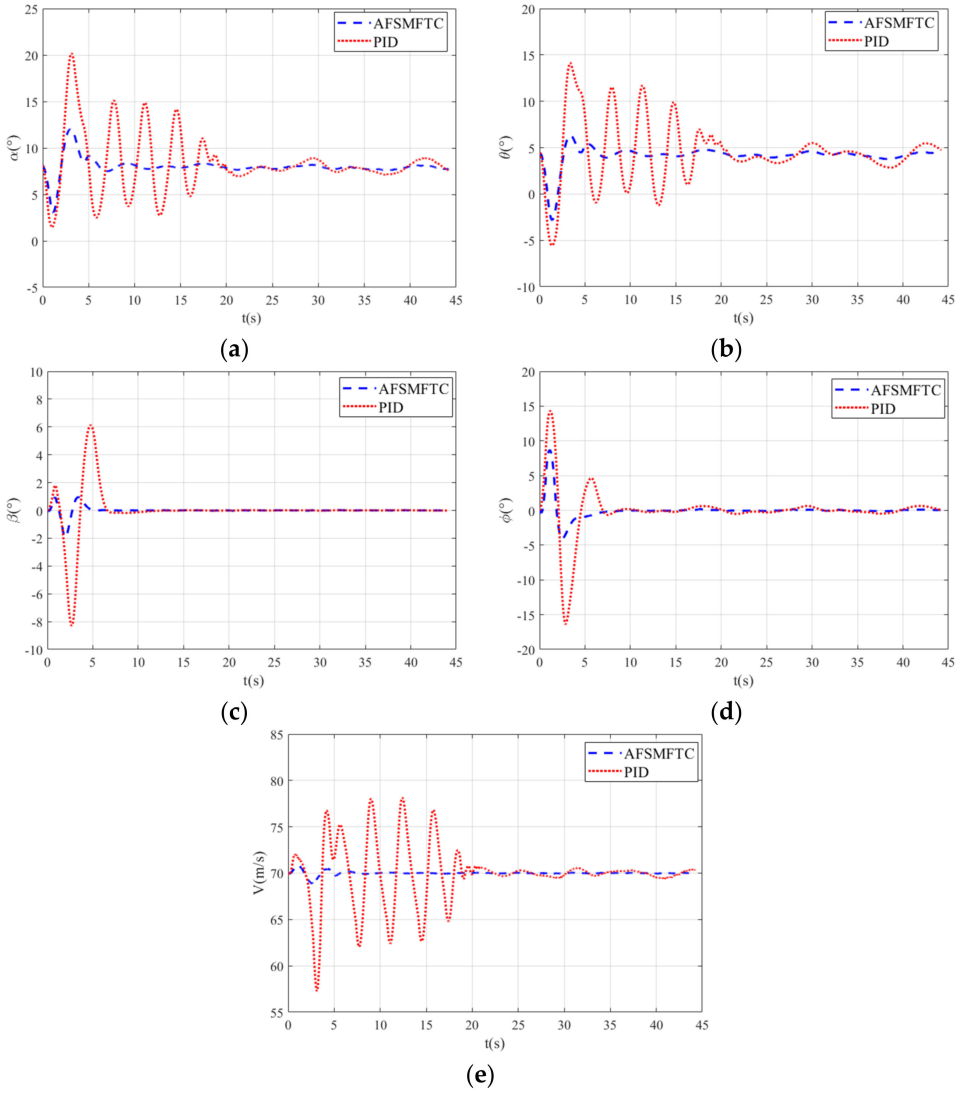


Figure 13. Response curves of flight variables of CBA under actuator faults: (**a**) Angle of attack; (**b**) Pitch angle; (**c**) Side-slip angle; (**d**) Roll angle; (**e**) Velocity.

Figure 12 shows that the conventional PID method leads to a sharp degradation in performance and violent fluctuations of path-tracking errors in the longitudinal and lateral directions after the introduction of the actuator efficiency loss fault. By contrast, the proposed AFSMFTC method compensates for the system faults in a timely and accurate manner and ensures real-time and accurate tracking for path commands under the control of adaptive laws, indicating good robustness.

Figure 13 shows the response curves of the system states of the CBA when its actuators experience efficiency loss. As can be seen, with the conventional PID method, the system state parameters oscillate, particularly so for α, θ and V. This shows that the conventional PID method cannot effectively guarantee system stability of the CBA under actuator faults, thereby seriously threatening the landing safety. By contrast, if a fault occurs, the designed AFSMFTC method can effectively keep the system state stable, thereby enhancing the fault-tolerant capability of the system.

6. Discussion

Compared with land-based landing, the glide landing of CBA is extremely complex and difficult because of the limited dimensions of the carrier deck, the impacts of the marine environment and the characteristics of the inverse manoeuvring zone. Consequently, it is the stage with the highest accident rate in CBA operational missions. To enhance the safety of CBA landings, scholars have conducted extensive research and achieved remarkable results [1–3,45,46]. However, there are some shortcomings in the related studies, primarily focused on the following three aspects.

Firstly, current researchers commonly use linear small disturbance models to design automatic landing systems for CBA [14,18,47,48]. In fact, there are significant disparities between linear model and the nonlinear model. Additionally, the landing environment is complex and highly variable, making it challenging to apply linear models effectively. Secondly, most studies were based on the hypothesis that CBA remains in their normal states without any faults [15,17,21,22]. whereas in reality, they are susceptible to combat damage and actuator faults due to complex flight environments and large variations in dynamic pressure in operational missions, leading to serious degradation of system performance and posing direct threats to landing safety. Thirdly, there is currently limited literature on fault-tolerant landing control for CBA, and the existing literature generally were focused on passive FTC, which can reduce the sensitivity of the controlled system to faults by enhancing the robustness of the controller [27,28]. Although neither fault diagnosis nor control reconstruction is needed, all types of possible faults must be known beforehand, which makes the controller relatively conservative and limited in its fault-tolerant function.

To address the aforementioned issues, this study proposes an active FTC strategy based on AFSMFTC. The strategy involves using an adaptive fuzzy network to conduct fuzzy approximation for the sliding-mode switching terms, and it effectively weakens the impacts of unknown disturbances on the control system without estimating the upper limit of perturbation. Adaptive laws are used to counter the actuator efficiency loss fault, automatically adjust the controller parameters in the light of actuator faults and complete FTC under fault conditions, and a sliding-mode controller is used to ensure CBA tracking along the expected flight path. Finally, the effectiveness of the proposed method is validated through multiple sets of comparative simulation experiments.

Currently, various advanced control theories such as fuzzy control and sliding-mode control have been gradually applied in the industrial field, playing a crucial role in driving technological development. In the future, with the improvement of the intelligent capabilities of naval forces worldwide, relevant carrier landing control strategies will also be widely promoted and applied.

7. Conclusions

To realise accurate and safe landing of CBA under actuator faults, an autonomous landing control system was designed in this study based on AFSMFTC. In the system, the

guidance subsystem comprising the longitudinal channel controlled by a path controller using a $\sigma - \beta$ filter and the lateral channel controlled by the PID method was designed to transform position errors into angular commands. APCS was designed to keep the velocity constant, and AFSMFTC, comprising an adaptive fuzzy network, adaptive laws and a sliding-mode controller, was designed to complete tracking and control for the attitude angle and fault compensation. The adaptive fuzzy network was shown to be effective at weakening the impacts of unknown disturbances on the control system through fuzzy approximation for the sliding-mode switching terms without estimating the upper limit of perturbation. The adaptive laws are used to counter the actuator efficiency loss fault, automatically adjust the controller parameters according to any fault condition and complete FTC under fault conditions, and the sliding-mode controller is used to ensure CBA tracking along the expected path. Furthermore, the Lyapunov function was used to theoretically analyse the disturbance compensation and FTC of the CBA, respectively, and it demonstrated uniform boundedness in the tracking errors of the closed-loop system. Finally, to verify the applicability of the AFSMFTC method, three different landing scenarios were simulated and compared. The simulation results showed that when the control system experiences actuator faults and unknown disturbances, the proposed AFSMFTC method is effective at countering them. Consequently, the landing accuracy and performance of the CBA are greatly improved compared to those with conventional control.

The fault-tolerant landing control technology for CBA is a challenging subject. This study specifically focuses on the research of fault-tolerant control technology under actuator efficiency loss fault. In future studies, it would be beneficial to investigate different types of faults in various scenarios. Additionally, it is crucial to consider the impact of sensor measurement errors on the landing control system of CBA. Researchers can pay attention to sensor accuracy, calibration methods, and the influence of environmental disturbances, while developing corresponding algorithms and techniques for filtering, calibrating, and detecting redundancies in sensor data. These efforts will enhance the robustness and reliability of the landing control system, ensuring safe and stable landings for carrier-based aircraft under various operating conditions.

Author Contributions: Conceptualization, Z.X. and J.A.; methodology, Z.X.; software, Z.X.; validation, Z.X.; formal analysis, Z.X.; investigation, Z.X.; resources, J.A.; writing—original draft preparation, Z.X.; writing—review and editing, Z.X.; visualization, Z.X. All authors have read and agreed to the published version of the manuscript.

Funding: This study was supported in part by the Shanghai Natural Science Fund under Grant No. 22ZR1404500.

Institutional Review Board Statement: Not applicable.

Informed Consent Statement: Not applicable.

Data Availability Statement: The data presented in this study are available on request from the corresponding author. The data are not publicly available due to the involvement of sensitive information about carrier-based aircraft in this research data.

Conflicts of Interest: The authors declare no conflict of interest.

References

1. Zhang, Z.B.; Zhen, Z.Y.; Jiang, J.; Xue, Y.X. Review on development in guidance and control of automatic carrier landing of carrier-based aircraft. *Trans. Nanjing Univ. Aeronaut. Astronaut.* **2018**, *50*, 734–744.
2. Zhen, Z.Y. Research development in autonomous carrier-landing/ship-recovery guidance and control of unmanned aerial vehicles. *Acta Autom. Sin.* **2019**, *45*, 669–681.
3. Xin, L.; Tang, Z.M.; Gai, W.Q.; Liu, H.B. Vision-based autonomous landing for the UAV: A review. *Aerospace* **2022**, *9*, 634. [CrossRef]
4. Duan, H.B.; Chen, L.; Zeng, Z.G. Automatic landing for carrier-based aircraft under the conditions of deck motion and carrier Airwake disturbances. *IEEE Trans. Aerosp. Electron. Syst.* **2022**, *58*, 5276–5291. [CrossRef]
5. Wang, Y.Q. Fixed-wing carrier-based aircraft: Key technologies and future development. *Acta Aeronaut. Astronaut. Sin.* **2021**, *42*, 525859.
6. Xia, X.; Bhatt, N.P.; Khajepour, A.; Hashemi, E. Integrated inertial-LiDAR-based map matching localization for varying environments. *IEEE Trans. Intell. Veh.* **2023**, *8*, 4307–4318. [CrossRef]

7. Xia, X.; Xu, R.S.; Ma, J.Q. Secure cooperative localization for connected automated vehicles based on consensus. *IEEE Sens. J.* **2023**, *23*, 25061–25074. [CrossRef]
8. Liu, W.; Xia, X.; Xiong, L.; Lu, Y.S.; Gao, L.T.; Yu, Z.P. Automated vehicle sideslip angle estimation considering signal measurement characteristic. *IEEE Sens. J.* **2021**, *21*, 21675–21687. [CrossRef]
9. Guo, Y.Y.; Chen, L.; Zhang, J. Research of a mixed robust PID/H_ Controller for UAV automatic landing under wind disturbance. *Fire Control Command* **2011**, *36*, 107–110.
10. Li, X.; Qu, X.Y.; Yuan, L.B. A nonlinear PID automatic landing controller based on PSO. *Comput. Simul.* **2009**, *26*, 73–76.
11. Deng, J.; Yan, Z.P.; Ai, J.L. Application of fuzzy control technology to automatic carrier landing system. *J. Syst. Simul.* **2012**, *24*, 645–650.
12. Zhou, D.P.; Zheng, Z.W.; Guan, Z.Y.; Ma, L. Barrier Lyapunov function based fixed-time control for automatic carrier landing with disturbances. *Proc. Inst. Mech. Eng. Part G* **2023**, *237*, 177–190. [CrossRef]
13. Guan, Z.Y.; Liu, H.; Zheng, Z.W.; Lungu, M.H.; Ma, Y.P. Fixed-time control for automatic carrier landing with disturbance. *Aerosp. Sci. Technol.* **2021**, *108*, 106403. [CrossRef]
14. Wang, L.P.; Zhang, Z.; Zhu, Q.D.; Wen, Z.W. Longitudinal automatic carrier-landing control law rejecting disturbances and coupling based on adaptive dynamic inversion. *Bull. Pol. Acad. Sci. Tech. Sci.* **2021**, *69*, e136217.
15. Sun, X.Y.; Jiang, J.; Zhen, Z.Y.; Wei, R.N. Adaptive fuzzy direct lift control of aircraft carrier-based landing. *J. Northwest. Polytech. Univ.* **2021**, *39*, 359–366. [CrossRef]
16. Meng, H.; Li, Y.-Z. Fuzzy controller design for automatic carrier landing of aircraft. In Proceedings of the 33th Chinese Control Conference, Nanjing, China, 28 July 2014.
17. Wang, L.P.; Jiang, X.-L.; Zhang, Z.; Wen, Z.X. Lateral automatic landing guidance law based on risk-state model predictive control. *ISA Trans.* **2022**, *128*, 611–623. [CrossRef]
18. Cui, K.K.; Han, W.; Liu, Y.J.; Wang, X.W.; Su, X.C.; Liu, J. Model predictive control for automatic carrier landing with time delay. *Int. J. Aerosp. Eng.* **2021**, *2021*, 8613498. [CrossRef]
19. Wang, W.Z.; Lv, M.W.; Yang, Y.T.; Zhang, S.Q.; Hu, J.W. Research on the technology of information fusion for the redundancy guidance for aircraft automatic carrier landing. In Proceedings of the 40th Chinese Control Conference, Shanghai, China, 26–28 July 2021.
20. Xu, J.W.; Zhang, K.P.; Zhang, D.F.; Wang, S.L.; Zhu, Q.; Gao, X.-G. Composite anti-disturbance landing control scheme for recovery of carrier-based UAVs. *Asian J. Control* **2022**, *24*, 1744–1754. [CrossRef]
21. Lungu, M.; Chen, M.; Vilcica, D.A. Backstepping- and sliding mode-based automatic carrier landing system with deck motion estimation and compensation. *Aerospace* **2022**, *9*, 644. [CrossRef]
22. Bhatia, A.K.; Ju, J.; Kumar, A.; Shah, S.A.A.; Rohra, A.; Zhen, Z.-Y. Adaptive preview control with deck motion compensation for autonomous carrier landing of an aircraft. *Int. J. Adapt. Control Signal Process* **2021**, *35*, 769–785. [CrossRef]
23. Bhatia, A.K.; Ju, J.; Zhen, Z.Y.; Ahmed, N.; Rohra, A.; Waqar, M. Robust adaptive preview control design for autonomous carrier landing of F/A-18 aircraft. *Aircr. Eng. Aerosp. Technol.* **2021**, *93*, 642–650. [CrossRef]
24. Milecki, A.; Nowak, P. Review of fault-tolerant control systems used in robotic manipulators. *Appl. Sci.* **2023**, *13*, 2675. [CrossRef]
25. Ding, Y.B.; Yue, X.K.; Chen, G.S.; Si, J.S. Review of control and guidance technology on hypersonic vehicle. *Chin. J. Aeronaut.* **2022**, *35*, 1–18. [CrossRef]
26. Fourlas, G.K.; Karras, G.C. A survey on fault diagnosis and fault-tolerant control methods for unmanned aerial vehicles. *Machines* **2021**, *9*, 197. [CrossRef]
27. Sun, J.G.; Song, S.M.; Wu, G.Q. Fault-tolerant track control of hypersonic vehicle based on fast terminal sliding mode. *J. Spacecr. Rocket.* **2017**, *54*, 1304–1316. [CrossRef]
28. Gao, Z.F.; Jiang, B.; Shi, P.; Liu, J.Y.; Xu, Y.F. Passive fault-tolerant control design for near-space hypersonic vehicle dynamical system. *Circ. Syst. Signal Process.* **2012**, *31*, 565–581. [CrossRef]
29. Vural, S.Y.; Dasdemir, J.; Hajiyev, C. Passive fault tolerant lateral controller design for an UAV. In Proceedings of the 18th International Federation of Automatic Control (IFAC) Conference on Technology, Culture and International Stability (TECIS), Baku, Azerbaijan, 13 September 2018.
30. Xie, M.L.; Wei, X.L.; Wang, H. Passive fault-tolerant control for control surface damage of UAV based on active disturbance rejection. *Tactical Missile Technol.* **2017**, *6*, 83–88+93.
31. Yang, W.Q.; Zhou, S.Y.; Lu, J.H. Research on fault tolerant control technology of carrier aircraft based on ESO compensation. *Electron. Opt. Control* **2023**, *30*, 28–34.
32. Raja, M.S.K.; Ali, Q. Recent advances in active fault tolerant flight control systems. *Proc. Inst. Mech. Eng. Part G* **2022**, *236*, 2151–2161. [CrossRef]
33. Salwa, Y.; Saida, B.; Abderrahim, K. Diagnosis and fault tolerant control against actuator fault for a class of hybrid dynamic systems. *Meas. Control* **2023**, *56*, 1240–1250. [CrossRef]
34. Ali, B.B.; Slim, D.; Faycal, B.H.; Anis, S. Adaptive sliding mode fault tolerant control design for uncertain nonlinear systems with multiplicative faults: Takagi-Sugeno fuzzy approach. *Proc. Inst. Mech. Eng. Part I* **2020**, *234*, 147–159.
35. Wang, Z.; Li, Q.; Li, S.R. Adaptive integral-type terminal sliding mode fault tolerant control for spacecraft attitude tracking. *IEEE Access* **2019**, *7*, 35195–35207. [CrossRef]
36. Yang, P.; Liu, P.; Wen, C.W.; Geng, H.L. Fault-tolerant control for a class of n-order systems based on fast terminal sliding mode and extended state observer. *Meas. Control* **2021**, *54*, 1234–1244. [CrossRef]

37. Huang, Y.H.; Qi, R.Y.; Jiang, B.; Tao, G. Adaptive failure compensation design for hypersonic vehicles based on dynamic surface backstepping control. *J. Univ. Sci. Technol. China* **2012**, *42*, 768–774.
38. Yao, Z.E.; Kan, Z.; Zhen, Z.; Shao, H.Y.; Li, D.C. Fault-Tolerant control for carrier-based UAV based on sliding mode method. *Drones* **2023**, *7*, 194. [CrossRef]
39. Xiao, H.Y.N.; Zhen, Z.Y.; Xue, Y.X. Fault-tolerant attitude tracking control for carrier-based aircraft using RBFNN-based adaptive second-order sliding mode control. *Aerosp. Sci. Technol.* **2023**, *139*, 108408. [CrossRef]
40. Zhen, Z.Y.; Jiang, S.Y.; Jiang, J. Preview control and particle filtering for automatic carrier landing. *IEEE Trans. Aerosp. Electron. Syst.* **2018**, *54*, 2662–2674. [CrossRef]
41. Duan, H.B.; Yuan, Y.; Zeng, Z.G. Automatic carrier landing system with fixed time control. *IEEE Trans. Aerosp. Electron. Syst.* **2022**, *58*, 3586–3600. [CrossRef]
42. Chakraborty, A.; Seiler, P.; Balas, G.J. Susceptibility of F/A-18 flight controllers to the falling-leaf mode: Linear analysis. *J. Guid. Control Dyn.* **2011**, *34*, 57–72. [CrossRef]
43. Feng, C.; Wang, Q.; Hu, C.H.; Gong, L.G. Active disturbance rejection attitude control for flapping wing micro aerial vehicle with nonaffine-in-control characteristics. *IEEE Access* **2020**, *8*, 20013–20027. [CrossRef]
44. Grondman, F.; Looye, G.H.N.; Kuchar, R.; Chu, Q.P.; Kampen, E.V. Design and flight testing of incremental nonlinear dynamic inversion-based control laws for a passenger aircraft. In Proceedings of the 2018 AIAA Guidance, Navigation, and Control Conference, Kissimmee, FL, USA, 8–12 January 2018.
45. Zhen, Z.Y.; Wang, X.H.; Jiang, J.; Yang, Y.D. Research progress guidance and control of automatic carrier landing of carrier-based aircraft. *Acta Aeronaut. Astronaut. Sin.* **2017**, *38*, 20435-1–20435-22.
46. Shen, L.C.; Kong, W.W.; Niu, Y.F. Ground-and ship-based guidance approaches for autonomous landing of UAV. *J. B. Univ. Aeronaut. Astronaut.* **2021**, *47*, 187–196.
47. Lu, J.H.; Yang, W.Q.; Zhou, S.Y.; Jiang, X. Research on LADRC based longitudinal landing deck tracking technology of carrier-based aircraft. *Flight Dyn.* **2022**, *40*, 9–15+23.
48. Huang, X.D.; Zhu, W.B.; Wen, Z.X.; Liu, W. Simulation and analysis of approach power compensation for automatic landing with carrier air wake. *Aero Weapon.* **2023**, *30*, 69–73.

Disclaimer/Publisher's Note: The statements, opinions and data contained in all publications are solely those of the individual author(s) and contributor(s) and not of MDPI and/or the editor(s). MDPI and/or the editor(s) disclaim responsibility for any injury to people or property resulting from any ideas, methods, instructions or products referred to in the content.